Journal of
Mechanical
Science and
Technology

Journal of Mechanical Science and Technology 21 (2007) 1937~1947

Toughness and fracture mechanisms of glass fiber/aluminum hybrid laminates under tensile loading

Sung-Choong Woo[1], Nak-Sam Choi[2,*] and Young-Wook Chang[3]

[1]*Department of Mechanical Design, Graduate School, Hanyang University, Seoul 133-791, Korea, Presently, Artificial Muscle Research Center, Konkuk University, 1 Hwayang-dong, Gwangjin-gu, Seoul 143-701, Korea*
[2]*Department of Mechanical Engineering, Hanyang University, 1271 Sa-1dong, Ansan-si, Kyunggi-do 426-791,Korea*
[3]*Department of Chemical Engineering, Hanyang University, 1271 Sa-3dong, Ansan-si, Kyunggi-do 426-791,Korea*

(Manuscript Received June 21, 2006; Revised August 7, 2007; Accepted Septemper 17, 2007)

Abstract

Tensile properties and fracture toughness of monolithic aluminum (Al), glass fiber reinforced plastics (GFRPs) and glass fiber/aluminum hybrid laminates (GFMLs) were examined in relation to the fracture processes of plain coupon and single-edge-notched specimens. Elastic modulus and ultimate tensile strength of GFMLs showed characteristic dependences on the kind of Al, fiber orientation and the Al/fiber layer composition ratio. Fracture toughnesses K_C and G_C of A-GFML-UD were comparable to those of GFRP-UD and were much superior to monolithic Al. However, GFML with a transverse crack parallel to the fiber layer deteriorated largely in toughness. Microscopic observation of the fracture zone in the vicinity of the crack tip revealed various modes of micro-cracks in the respective layers as well as fiber fractures and delamination between fiber/Al layers. Such damage advances in GFMLs dependent on the orientation of the fiber layer and the Al/fiber composition ratio strongly influenced the strength and toughness of GFMLs.

Keywords: Glass fiber aluminum hybrid laminates; Tensile behavior; Fracture process; Delamination

1. Introduction

In the early 1980s, fiber metal laminates (FMLs) were developed for aeronautical materials in an attempt to obtain the combined merits of the constituent's aluminum alloy (Al) and conventional fiber reinforced plastic (FRP) composites. FMLs [1-4] consisting of alternating layers of unidirectional fiber-reinforced plastics laminae and thin Al alloy sheets have outstanding mechanical properties in comparison to either conventional FRPs or Al alloys. FMLs have attracted considerable interest as promising industrial materials on account of their high specific strength and specific stiffness as well as high resistance against environmental aging [5-7]. However, FMLs show rather weak toughness against delamination due to the occurrence of local cavities in the FRP layer during the curing process, and to the formation of residual stress caused by their different thermal contractions between the Al and fiber layers. Although some kinds of FMLs are commercially available by the trade name of GLARE [8, 9] or ARALL [10-14] their fracture characteristics and mechanisms associated with the Al kind, notch existence and fiber orientation are not sufficiently verified as far as the authors know. Recently, the studies on FMLs have mainly focused on fatigue or impact characteristics of FMLs whose constituent fiber layer was unidirectional [8, 9, 13, 14]. To apply FMLs in automobile components and infrastructures, further studies in relation to basic mechanical properties and fracture toughness of FMLs with various lay-up angles should be carried out for their safety, integrity and reliability. Present authors reported acoustic emission (AE) characteristics of Al, glass fiber reinforced plastics

*Corresponding author. Tel.: +82 31 400 5283, Fax.: +82 31 406 5550
E-mail address: nschoi@hanyang.ac.kr

(GFRP) and GFMLs in relation to their macroscopic and microscopic fracture processes [15-17].

The purpose of this work was to experimentally clarify effects of various lay-up sequences and Al/fiber composition ratios on the tensile properties and fracture toughness of monolithic Al, GFRP and GFMLs. Single-edge-notched (SEN) specimens were used for observing the behaviors of crack initiation and propagation around the initial notch tip during the tensile test. After the test, a thinned specimen was prepared by the thin sectioning technique [18] for polarized optical microscopic observation of the fracture mechanisms of GFMLs. A scanning electron microscope (SEM) was also employed for the microscopic identification of fracture surfaces.

2. Experimental

2.1 Materials and specimen preparation

Table 1 presents the various materials used for this study, specimen designations and their lay-up stacking sequences. Two kinds of monolithic Al sheets (Al 1050, Al 5052) with a thickness of 0.5 mm and unidirectional glass fiber/epoxy prepreg (UGN150, SK Chemical) with a thickness of 0.125 mm were employed for the manufacturing of the GFML panels. Two kinds of lay-up composition ratios (2/1 and 3/2) were adopted for GFMLs (as shown in Fig. 1). Specimens with a lay-up composition ratio of 2/1 and 3/2 are designated as A-GFML and B-GFML, respectively. Specimen length direction was in accordance with the rolling direction of the monolithic Al sheet for all GFMLs specimens. To obtain good adhesion ability between monolithic Al and glass fiber/epoxy prepregs, a pretreatment of phosphoric acid anodizing (PAA) for one hour was performed on the surface of the monolithic Al sheets. Adhesive film (Bondex206, Hankook Fiber Co.) with a thickness of about 200 μm was inserted between the Al sheet and glass fiber prepreg by using a hand lay-up procedure. GFRP and GFML panels were cured in an autoclave by using a thermal cycle recommended by the prepreg manufacturer.

Fig. 2 shows schematics of the tensile specimen of Al, plain coupon type specimen of GFRP and GFML according to the JIS K7075 [19]. A single-edge-notch (SEN) was introduced with care by using a low-speed diamond wheel cutter (ISOMET, Buehler Co.). The initial notching direction was perpendicular to the specimen length. After that, a sharp notch was further introduced by pushing a fresh razor blade into the initial notch tip. The notch depth and width were kept to 12.6 and 0.3 mm, respectively. Fig. 3 shows an enlarged view of the initial crack tip introduced by a

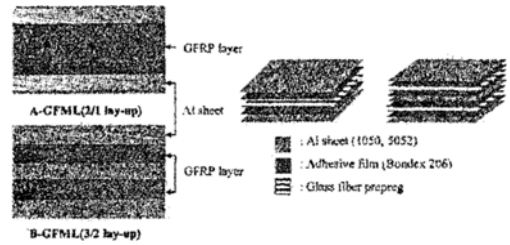

Fig. 1. Schematic of fabricated GFMLs and lay-up composition ratio.

Table 1. Designation of Al materials and their composites used in this study.

Materials	Specimen designation	Stacking sequence
Monolithic aluminum	Al 1050	-
	Al 5052	-
Glass fiber reinforced plastics	GFRP-UD	$[0^\circ_{16}]$
	GFRP-CP	$[0^\circ_4/90^\circ_8/0^\circ_4]$
	GFRP-90	$[90^\circ_{16}]$
Glass fiber/ aluminum hybrid laminates	A-GFML-UD	$[Al/0^\circ_8/Al]$
	A-GFML-CP	$[Al/0^\circ_2/90^\circ_4/0^\circ_2/Al]$
	A-GFML-90	$[Al/90^\circ_8/Al]$
	B-GFML-UD	$[Al/0^\circ_2/Al/0^\circ_2/Al]$
	B-GFML-CP	$[Al/0^\circ/90^\circ/Al/90^\circ/0^\circ/Al]$
	B-GFML-90	$[Al/90^\circ_2/Al/90^\circ_2/Al]$

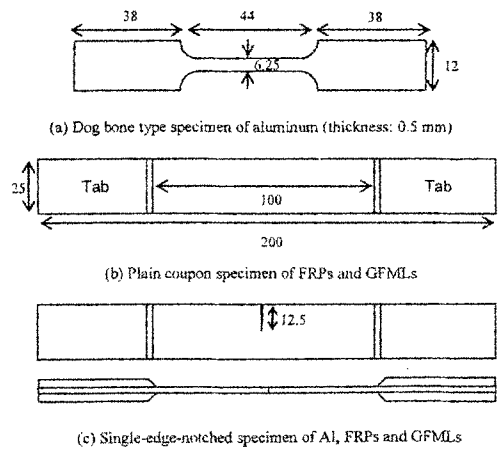

Fig. 2. Schematic of monolithic aluminum, GFRP, and GFMLs specimens for tensile test. (a) dog bone type specimen of Aluminum, (b) plain coupon specimen of GFRP and GFMLs and (c) single-edge-notched specimen of Al, GFRP and GFMLs (unit: mm).

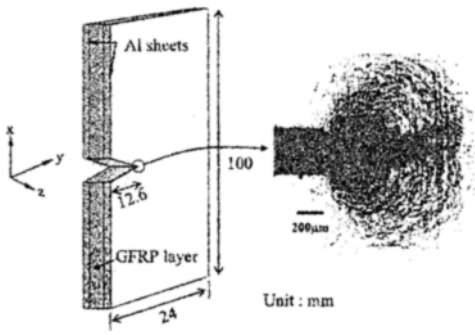

Fig. 3. Schematic of a single-edge-notched specimen. Right photo shows an enlarged view of an initial crack tip introduced by a sharp razor blade.

sharp razor blade. Some compressive damage formed in the Al skin behind the crack tip, while no damage was seen in front of the crack tip.

2.2 Tensile test and fractography

For plain coupon specimens, tensile stress-strain curves were measured with a crosshead speed of 0.5 mm/min, with a universal test machine (Zwick 250). For each kind of test, five specimens were tested. Strain was measured through an extenso-meter with a gauge length of 40 mm placed on the center portion of the specimen.

For SEN specimens, load (P)-displacement (δ) curves were obtained with a crosshead speed of 0.1 mm/min. Crack initiation and propagation behaviors in front of the initial notch tip were observed through the traveling microscope during the tensile test. After the test was finished, specimens for transmission optical observation were polished to make thin specimens with a thickness of about 250 μm by utilizing the thin section technique [18]. The state of damage around the crack tip was examined under reflected and transmitted light with a polarized optical microscope. Fracture surfaces of GFRP and GFML were also observed with a scanning electron microscope (SEM).

2.3 Data reduction of critical stress intensity factor K_C

The mode I critical stress intensity factor K_{IC} is generally utilized as a fracture mechanics parameter applicable to the linear elastic isotropic materials with a crack under opening load. Values of K_{IC} can be measured by using the following relationship (1) [20, 21] adopting a linear elastic fracture mechanics (LEFM) analysis of the single-edge notched tensile specimen.

$$K_C = f(a/W)\frac{P_Q}{B\sqrt{W}} \tag{1}$$

where a is the initial crack length, B the specimen thickness, W the specimen width and f(a/W) the dimensionless function of a/W given in polynomial as Eq. (2).

$$f(a/W) = \frac{\sqrt{2\tan\frac{\pi a}{2W}}}{\cos\frac{\pi a}{2W}}[0.75 + 2.02(\frac{a}{W}) + 0.371 + (1-\sin\frac{\pi a}{2W})^3] \tag{2}$$

The critical load P_Q is determined by the load corresponding to the crack initiation point.

It has been reported that the fracture parameter of K_{IC} offered an internally consistent measure of toughness K_C as a global fracture evaluation index including different types of local crack propagation in anisotropic composite materials [22-25]. We assumed the LEFM analysis of Eq. (1) for the fracture evaluation of these types of hybrid composites. From the P-δ curves of Al, GFRP and GFML specimens containing a single-edge notch, K_C is measured according to the ASTM standard [21]. The intercept load $P_{5\%}$ of the 5 % offset line with the P-δ curve was adopted to be P_Q such that the ratio of the maximum load P_{max} to $P_{5\%}$ is lower than 1.1 P_Q. Otherwise, the first peak load in the P-δ curve represented P_Q.

2.4 Data reduction of critical energy release rate G_C

The strain energy release rate G may postulate the elastic-plastic fracture behavior. It is assumed that the fracture mechanics parameter G may also be a consistent measure of the global fracture toughness of anisotropic composite materials interpreted by various types of local crackings as shown in several references [22-25]. Its critical value G_C is determined by Eq. (3) [26]

$$G_C = \frac{U}{BW\phi} \tag{3}$$

where the stored energy U is the area bounded by P-δ curve and the δ axis up to P_Q. The energy calibration factor ϕ is calculated through Eq. (4), a function of a/W and specimen geometry reflecting the change of compliance C.

$$\phi = \frac{C}{dC/d(a/W)} \tag{4}$$

3. Results and discussion

3.1 Tensile performance analysis of GFMLs

3.1.1 Effects of PAA pretreatment and rolling direction on tensile behavior of monolithic aluminum alloy

Typical stress-strain curves of untreated and PAA treated aluminum alloys (Al 1050 and Al 5052) in the rolling direction are shown in Fig. 4. The initial stage of each curve shows a similar linear elastic behavior until a yield strain around 0.5 %. During further strain from 1 to 4~8 %, a considerable increase of stress to the maximum appears for Al 1050, whereas there is very little increase in Al 5052. After passing the maximum the apparent stress diminished rapidly. On the contrary, PAA pretreatment caused some amount of decrease in failure strain.

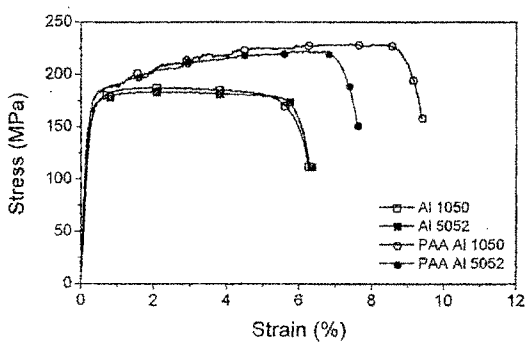

Fig. 4. Typical stress-strain relationships of Al1050 and Al5052, tested in the rolling direction.

Table 2. Tensile properties of monolithic aluminum plates in parallel with/transverse to the rolling direction. PAA-Al indicates PAA-treated aluminum.

Materials	Young's modulus, E (GPa)	Ultimate tensile strength, σ_{UTS} (MPa)	Failure strain, ε_f (%)
Al 1050	69/69	195±2.3 / 181±3.3	6.4±0.6 / 5.4±0.1
PAA-Al 1050	69/69	193±4.8 / 185±2.4	6.4±1.8 / 5.6±0.5
Al 5052	70/70	229±0.7 / 221±2.7	9.5±0.3 / 10.2±0.8
PAA-Al 5052	70/70	223±2.2 / 225±3.1	7.6±0.5 / 7.8±0.9

Results of tensile properties of the Al sheets in the direction parallel and transverse to the rolling are listed in Table 2. For Al 1050 the ultimate tensile strength (σ_{UTS}) and the failure strain (ε_f) in the rolling direction are larger than those in the transverse direction. Al 5052 in the rolling direction shows larger σ_{UTS} and less ε_f in comparison to the transverse direction. The pretreatment of Al 1050 and Al 5052 by PAA caused deterioration within 3 % in σ_{UTS} and ε_f, except for a 20 % reduction in ε_f of Al 5052. Such differences of tensile properties of Al alloys according to the rolling direction and pre-treatment should have influences on the fracture characteristics of fiber/aluminum hybrid laminates.

3.1.2 Effects of fiber orientation on tensile behavior of GFRP

Fig. 5 shows the typical stress-strain curves of GFRP specimens. The GFRP-UD specimen whose loading direction was the same as its fiber orientation shows almost a linear elastic behavior without yielding until the final fracture, whereas GFRP-CP and GFRP-90 specimens exhibit an yielding behavior such as some change in the slope at strain 0.5 % and 0.13 %, respectively. This is reasonable in that brittle glass fibers for GFRP-UD supported most of the applied load, while epoxy matrix parts for GFRP-CP and GFRP-90 substantially sustained the applied load. As presented in Fig. 6, GFRP shows very high anisotropy in elastic modulus and σ_{UTS} according to fiber orientation. Values of σ_{UTS} for GFRP-UD are 16 times higher than those of GFRP-90.

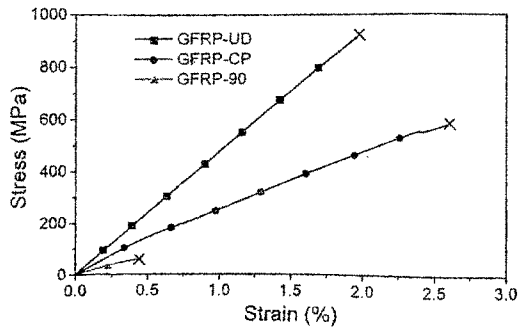

Fig. 5. Typical stress-strain curve of GFRP.

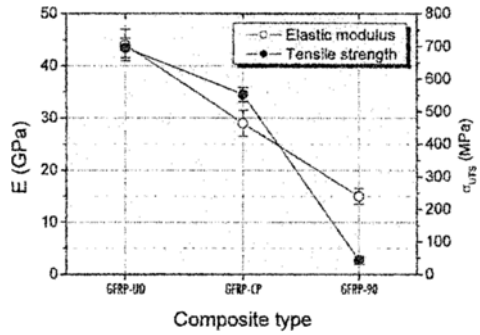

Fig. 6. Elastic modulus and ultimate tensile strength of GFRP.

3.1.3 Tensile performances of GFMLs according to fiber orientation and fiber/Al composition ratio

Stress-strain curves of Al 1050-based and Al 5052-based GFML specimens are shown in Fig. 7. Some marks of 'x' in the figure indicate a sudden load drop or pop-in point. In both cases, tensile stress behaviors with increasing strain were divided into three stages: the first stage of the initial linear elastic behavior, the second stage of the yielding behavior with some decrease in the slope, and the third stage showing some linear relationship again until a sudden load drop by the fracture. Kawai et al. [27] reported that the yielding stage in the stress-strain curve of commercial product GLARE2 in the fiber direction corresponded to the yielding point of the monolithic Al layer. In this study, however, the slope change for each GFML began somewhat earlier than the yielding strain of 0.5 % for the monolithic Al sheet. The earlier yielding behavior can be explained on the basis of the thermally induced residual stresses formed in the high temperature (125°C) cure process of GFML fabrication. Due to the higher thermal expansion coefficient (about 23 μm/m°C) of the Al layer than that (about 11 μm/m°C in the longitudinal direction) of the GFRP-UD layer there existed relatively high tensile residual stresses thermally induced in the Al layer of GFML-UD at room temperature, while the GFRP layers had to be under compressive residual stresses. With an application of the tensile load to the GFML-UD, the thermally induced tensile residual stress should be added to an apparent tensile stress which was mechanically induced in the Al layer by the loading rig. Thus, the tensile residual stress in the Al layer caused the earlier yielding of the Al layer itself, which resulted in the earlier global yielding of GFML-UD. Earlier yielding of GFML-90 can be also explained by the higher thermal expansion coefficient (about 60

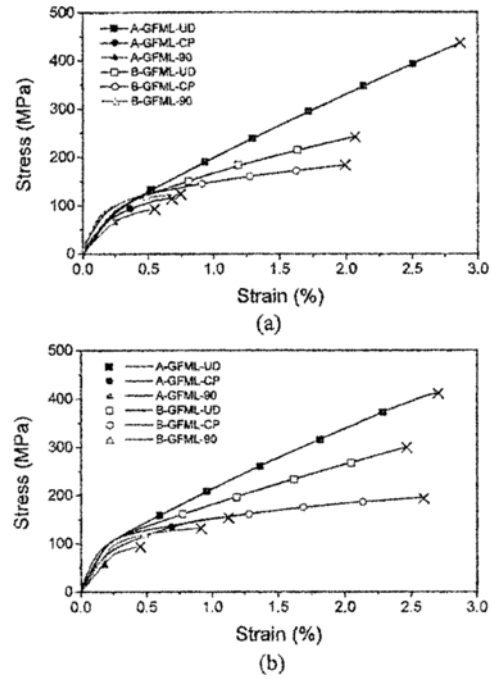

Fig. 7. Typical stress-strain curves of (a) Al 1050 based and (b) Al 5052 based GFML specimens.

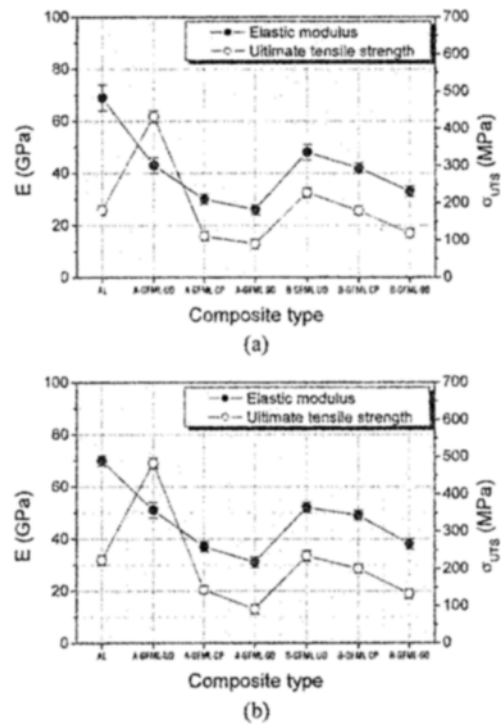

Fig. 8. Elastic modulus (E) and ultimate tensile strength (σ_{UTS}) for monolithic Al and various GFML specimens: (a) Al 1050 base GFML and (b) Al 5052 base GFML.

μm/m°C in the transverse direction) of the GFRP-90 layer than that of the Al layer. In this case relatively high tensile residual stresses were thermally induced in the GFRP-90 layer at the room temperature. Thus, the global yielding strain of GFML-90 was shown to be quite less than the failure strain of about 0.45% for the GFRP-90 sheet (see the failure strain of GFRP-90 in Fig. 5).

Fig. 8 shows elastic modulus (E) and σ_{UTS} for various GFML specimens. Elastic moduli for the respective GFMLs basically conformed, but were inferior by 5-12 % to the results calculated from the rule of mixture considering the modulus values in the corresponding direction of Al and fiber layers. For example, the elastic modulus of A-GFML-UD was measured around 51 GPa, while it was calculated to be 57 GPa according to the rule of mixture for 50 %/50 % volume fractions of GFRP-UD (E=44 GPa) and Al (E=70 GPa). This may be due to the low modulus of the adhesive film layers inserted between Al and fiber layers in GFMLs and to the various stress distributions applied to the respective layers of GFMLs.

For both cases of Al1050 and Al5052, σ_{UTS} of A-GFML-UD was the supreme, 2.2 and 2.4 times higher than that of the corresponding monolithic Al sheet, respectively. GFML-CP and -90 specimens showed rather lower σ_{UTS}. σ_{UTS} for various GFMLs did not conform to the rule of mixture, suggesting different characteristics in the fracture behavior according to the orientation of the fiber layer, the Al/fiber composition ratio and the kind of Al.

3.2 Fracture toughness analysis of GFMLs

3.2.1 Effects of fiber orientation and fiber/Al composition ratio on K_C

Fig. 9 shows the values of K_C for GFRP and GFML specimens. K_C values of Al 5052 based GFMLs were consistently higher than those of Al 1050 based ones. Although the overall variational behavior of K_C for GFMLs according to the composite types was similar to that of σ_{UTS} for un-notched ones in Fig. 8, σ_{UTS} of A-GFML-UD was lower than that of GFRP-UD (see Fig. 5) while K_C for the A-GFML-UD specimen was rather a bit higher than that of GFRP-UD. K_C of the A-GFML-UD specimen whose fiber orientation was perpendicular to the initial notch was the supreme, almost 2 times as high as that of monolithic Al. A-GFML-90 showed 4.6 times higher K_C than GFRP-90, but was lower by 56 % than

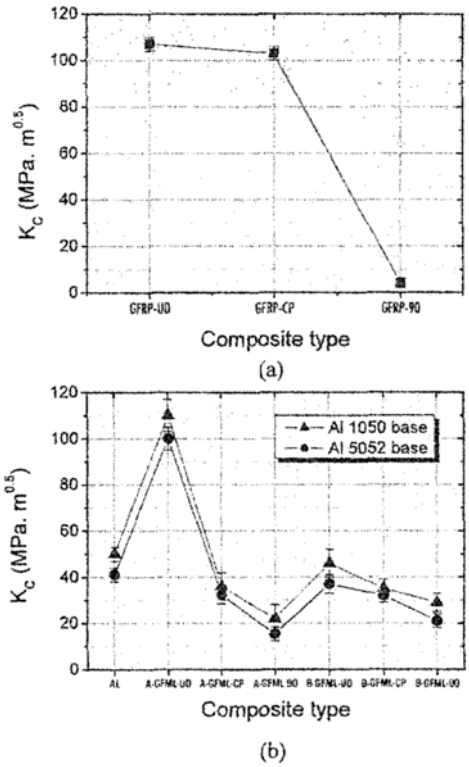

Fig. 9. Critical stress intensity factor K_C for (a) GFRP and (b) GFML composite specimens.

monolithic Al. This can be because the Al layers having high K_C values of 40-52 MPa$\sqrt{m}$ hindered cracking in the fiber layer with 90° fibers. The high K_C values of the Al layers resulted in higher K_C of B-GFML-90 by 30 % than that of A-GFML-90.

3.2.2 Effects of fiber orientation and fiber/Al composition ratio on G_C

The overall behavior of G_C for the GFML specimens according to composite type had a similar tendency to that of K_C, as shown in Fig. 10. The superiority in G_C for A-GFML-UD was obvious and was about 4.5 times higher than that of monolithic Al. B-GFML-UD revealed an improvement by 26 % in G_C. However, A-GFML-90 showed a degraded G_C lower by 21 % but 27 times higher than GFRP-90. Considering that G_C indicates basically the stored energy U for a cross-sectional area BW in Eq. (6), a large formation of the plastic deformation region for GFML specimens shown in Fig. 7 caused such superiority in G_C. Thus, it is to be noted that G_C of A-GFMLs was largely influenced according to the fiber orientation and Al/fiber composition ratio. The extents of their

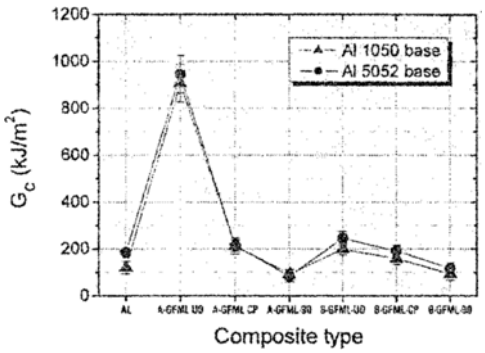

Fig. 10. Critical energy release rate G_C for GFML composite specimens.

influences on G_C were much greater than those on K_C.

3.2.3 Characteristic fracture mechanisms of various GFMLs

The representative fracture mechanisms of fiber reinforced plastics (FRPs) are matrix cracking, ply delamination and fiber breakages. In case of FMLs, plastic deformation of Al layers as well as delamination between fiber and Al layers should additionally occur.

Transmission optical micrographs of micro-fracture behaviors of only the fiber layers in the vicinity of the initial crack tip of the GFRP-UD, A-GFML-UD and B-GFML-UD specimens at the maximum load are shown in Fig. 11. Thin specimens with a thickness of about 200 μm for optical observation were made by using the thin sectioning and surface polishing techniques after the removal of the Al layer by a low-speed diamond wheel cutter. For GFRP-UD (Fig. 11(a)), although some amount of fiber breakage was induced ahead of the notch tip, the crack could not propagate across the 0° fiber layer with high strength. Thus, shear cracking was initiated perpendicular to the notch, which was propagated in the fiber length direction, i.e., in the weakest direction of the fiber layer inducing the fracture mode change. Similar fracture patterns were observed in A-GFML-UD (Fig. 11(b)). Such fracture behaviors were confirmed by an acoustic emission (AE) analysis of A-GFML-UD [15-17] in that a drastic increase in AE event rate and amplitude arose during the initial stage of the fracture mode change, indicating some fiber breakage in the fiber layer and then partial delamination between Al and fiber layers, instead of the tensile crack propagation. The high hindrance effect of the fiber layer against the tensile cracking brought about the high

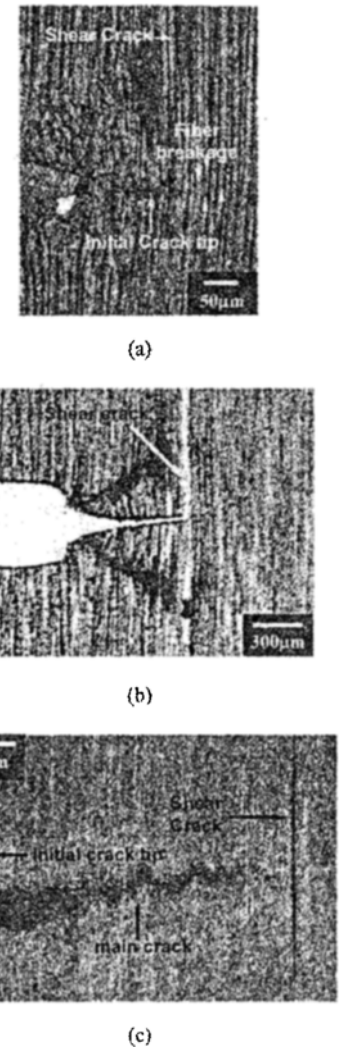

Fig. 11. Optical micrographs in the vicinity of the crack tip in the fiber layer of various single edge notched GFMLs at the maximum load: (a) GFRP-UD, (b) A-GFML-UD and (c) B-GFML-UD specimens.

Fig. 12. Scanning electron micrograph taken from the fracture surface of the fiber layer of a single edge notched A-GFML-90 specimen.

value of K_C and G_C in Figs 9 and 10. On the other hand, in the case of B-GFML-UD, whose composition ratio of 0° fiber layer was about 2/5, much smaller than that of A-GFML-UD (see Fig. 1), the main crack initiated in a shear mode but propagated in a major mode of tension showing a zigzagged fracture across the 0° fiber layer and sometimes generating fiber breakages and shear cracks.

Fig. 12 shows SEM observation of the fracture surface of the fiber layer of the A-GFML-90 specimen. The fiber orientation parallel to the initial notch guided the main crack to propagate along the initial notch direction, resulting in lower K_C and G_C than those of the Al alloy sheet. The toughness of the neighboring Al layer caused a stable propagation of the crack. Some amount of fibers bridged across the upper and lower fracture surfaces (see arrows) as well as the rugged formation of the fracture surface might have brought about a small improvement in K_C and G_C.

Fig. 13 shows microscopic thickness-wise views (upper photos) at the opposite edges of various GFML specimens after the test and the corresponding crack path (lower photos) in the Al skin layer. For A-GFML-UD (Fig. 13(a)), a large delamination occurred with a cohesive fracture in the adhesion film layer between the Al skin and fiber core layers under the influence of shear crack propagation in the 0° fiber core layer perpendicular to the initial notch, as well as a tensile crack advance in the Al skin layer in the notching direction. However, for A-GFML-CP (Fig. 13(b)) whose fiber layer had a cross-ply structure, zigzag fracture of the 0° fiber ply, tensile cracks in the 90° fiber ply, ply delamination between 0° and 90° fiber plies and delamination between Al skin and fiber core layers were observed. For A-GFML-90 (Fig. 13(c)), the main crack propagated in the notch direction through the transverse matrix cracks of the 90° fiber core layer. Local plastic deformation of the Al skin layer around the propagating crack tip as well as only a small amount of delamination between the Al and fiber layers was observed. It should be noted that the initial tensile crack in the Al layers propagated almost straight forward, irrespective of fiber orientation and the Al/fiber composition ratio. Those fracture processes in various GFMLs were also confirmed by classifying and analyzing the characteristics of the event rate and amplitude data of AE signals [15-17]. B-GFML-UD (Fig. 13(d)) with a high composition ratio (3/5) of the Al layer showed a rather suppressed zigzag fracture in the 0° fiber layers and a limited delamination between the Al and fiber layers which seemed to cause the full propagation of the main crack.

The characteristic fracture processes of the various GFML specimens strongly dependent on fiber orientation and the fiber/Al composition ratio are schematically shown in Fig. 14. With the exception of A-

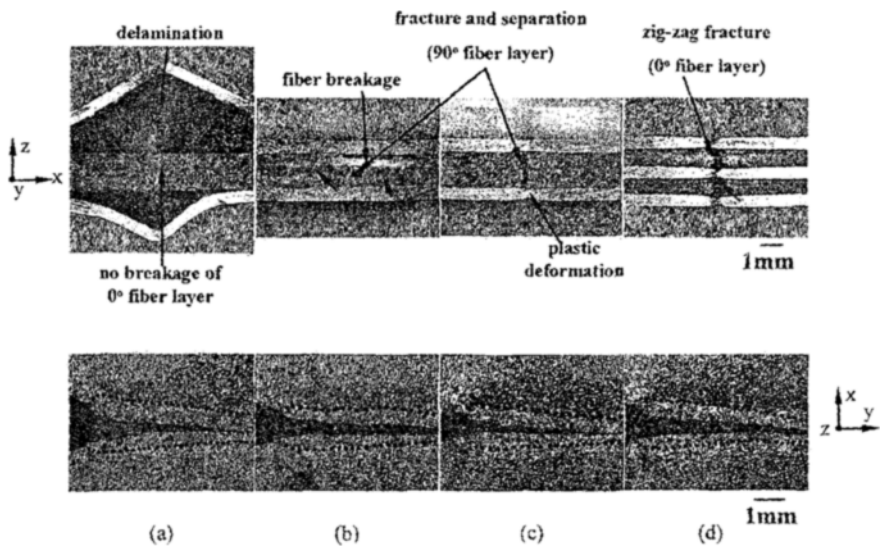

Fig. 13. Microscopic thickness-wise views (upper) and propagating crack behavior (lower) of various GFML specimens after the tensile test. Dotted lines indicate boundaries of plastic deformation zone around the propagating crack: (a) A-GFML-UD, (b) A-GFML-CP, (c) A-GFML-90 and (d) B-GFML-UD.

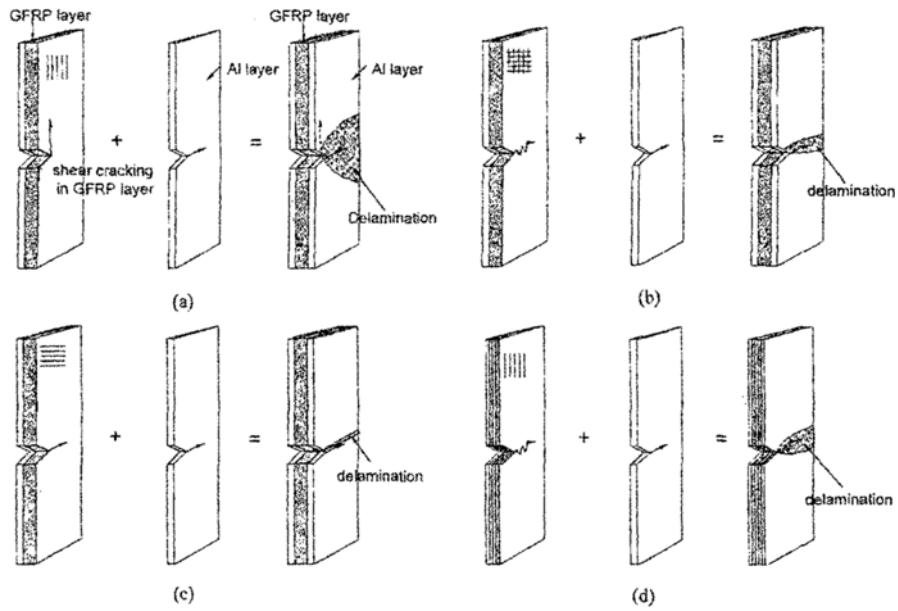

Fig. 14. Schematics of various crack propagation behaviors depending on fiber orientation and fiber/aluminum composition ratio: (a) A-GFML-UD, (b) A-GFML-CP, (c) A-GFML-90 and (d) B-GFML-UD.

GFML-UD, cracks propagated almost in parallel with the initial notch direction (see Fig. 14(b)-(d)). In the case of A-GFML-UD (Fig. 14(a)); however, the initial tensile crack changed its path as a shear mode inducing a large amount of delamination while approaching P_{max}. Such delamination as illustrated in Fig. 14(a) became a significant fracture mode requiring an additional load and/or energy absorption in its mechanical failure behaviors of A-GFML-UD. It is thus thought that the experimental test results shown in Figs. 9(b) and 10 obtained by using Eq. (1) had some over-estimated values higher than the true mode I toughnesses K_{IC} and G_{IC} of A-GFML-UD.

4. Conclusions

Tensile properties and fracture toughnesses of K_C and G_C for plain coupon and single-edge-notched specimens of Al, GFRP and GFMLs have been evaluated in association with fracture processes. The fracture state around the crack tip was examined with a reflection and transmission optical microscope. Fracture surfaces of GFRP and GFMLs were also observed by a scanning electron microscope (SEM). The results obtained are summarized as follows:

(1) Elastic modulus of GFMLs basically conformed to the rule of mixture of Al and fiber layers. Ultimate tensile strength of GFMLs largely depended on fiber orientation. Their tensile deformation behaviors showed initially an elastic stage due to the elastic behavior of both Al and fiber layers and then a yielding and plastic stage due to the plastic deformation behavior of Al layers.

(2) Fracture toughness of A-GFML-UD whose fiber orientation was perpendicular to the initial notch was comparable to that of GFRP-UD and much higher by 100-400 % than that of its constituent Al layer.

(3) From the microscopic observation various crack propagation behaviors of the GFMLs were schematically modeled: the main crack in A-GFML-UD did not propagate in the transverse direction through the fiber layer and instead caused a large delamination between fiber and Al layers. However, GFML-90 showed a straight propagation of crack thus bringing about a drastic decrease in toughness. Such types of crack advances varied not only with the orientation of fiber layers but also with the composition ratio of Al layers in GFMLs. The characteristic fracture behaviors largely affected the ultimate tensile strength as well as fracture toughness of GFMLs.

Acknowledgements

This work was supported by grant No. R01-2005-000-10566-0 from the Basic Research Program of the

Korea Science & Engineering Foundation as well as by the 2nd Brain Korea 21 Project from the Korea Research Foundation.

References

[1] R. Marissen, Flight simulation behavior of aramid reinforced aluminum lamiantes (ARALL), Engineering Fracture Mechanics. 43 (1984) 261-277.

[2] J. B. Young, J. G. Landry and V. N. Cavoulacos, Crack growth and residual strength characteristics of two grades of glass-reinforced aluminum GLARE, Composite Structures. 27 (1994) 457-469.

[3] A. Asundi and Y. N. Alta, Fiber metal laminates: an advanced material for future aircraft, Journal of Materials Processing Technology. 63 (1997) 384-394.

[4] M. Kawai, M. Morishita, S. Tomura and K. Takumida, Inelastic behavior and strength of fiber-metal hybrid composite: GLARE, International Journal of Mechanical Sciences. 40 (1998) 183-198.

[5] H. Parvatareddy, P. H. Wilson and D. A. Dillard, Impct damage resistance and tolerance of high-performance polymeric composites subjected to environmental aging, Composites Science and Technology. 56 (1996) 1129-1140.

[6] K. Liao, C. R. Schultheisz and D. L. Hunston, Effects of environmental againg on the properties of pultruded GFRP, Composites Part B. 30 (1999) 485-493.

[7] M. M. Thwe and K. Liao, Effects of envrionmental aging on the mechanical properties of bamboo-glass fiber reinforced polymer matrix hybrid compoposites, Composites Part A. 33 (2002) 43-52.

[8] H. Yan, R. Ren, C. Tao and H. Li, Fatigue Crack initiation in fibre-metal laminate GLARE 2, Materials Science and Engineering A. 234-236 (1997) 621-624.

[9] D. J. Shim, R. C. Alderliesten, S. M. Spearing and D. A. Burianek, Fatigue crack growth prediction in GLARE hybrid laminates, Composites Science and Technology. 63 (2003) 1759-1767.

[10] J. S. Hidde and C. T. Herakovich, Inelastic response of hybrid composite laminates, Journal of Composite Materials. 26 (1992) 2-19.

[11] H. Yan, C. Tao and H. Li, Study on arall failure behavior under tensile loading, Scripta Materialia. 35 (1996) 1379-1384.

[12] J. L. Chen and C. T. Sun, Modeling of orthotropic elastic-plastic properties of ARALL laminates, Composites Science and Technology. 36 (1989) 321-337.

[13] R. O. Ritchie, W. Yu and R. J. Bucci, Fatigue crack propagation in ARALL laminates: measurement of the effect of crack-tip shielding from crack briding, Engineering Fracture Mechanics. 32 (1989) 361-377.

[14] J. Macheret and J. L. Teply, Delamination shape effects in aramid-eposy-aluminum (ARALL) lamiantes with fatigue cracks, Polymer Composites 10 (1989) 322-327.

[15] S. C. Woo and N. S. Choi, A study on fracture behaviors of single-edge-notched glass fiber/aluminum laminates using acousitc emission, Transactions of KSCM(in Korean). 18 (2005) 1-12.

[16] S. C. Woo and N. S. Choi, Acoustic emission characteristics during fracture process of glass fiber/aluminum hybrid lamninates, Transactions of KSNT(in Korean). 25 (2005) 274-286.

[17] S. C. Woo, D. J. Kim and N. S. Choi, Acoustic emission characteristics of single-edge-notched glass fiber/aluminum hybrid laminate, Key Engineering Materials. 306 (2006) 19-24.

[18] N. S. Choi and K. Takahashi, Microscopic observation of failure in polymer-matrix composites under reflected and transmitted light, Journal of Materials Science Letters. 12 (1993) 1718-1721.

[19] JIS K 7054, Testing Method for Tensile Properties of Glass Fiber-Reinforced Plastics, Japanese Industrial Standards Committee, (1987).

[20] H. Tada, P. C. Paris and G. R. Irwin, The Stress Analysis of Cracks Handbook, Paris Production Inc., (1985).

[21] ASTM E 399-83, Standard Test Method for Plane-Strain Fracture Toughness of Metallic Materials, American Society for Testing and Materials, (1993).

[22] P. J. Hinne, B. Brew, R. A. Duckett and I. M. Ward, The fracture behavior of carbon fibre reinforced poly(ether ether ketone), Composites Science and technology. 33 (1988) 35-48.

[23] P. J. Hinne, B. Brew, R. A. Duckett and I. M. Ward, Failure mechnisms in continuos carbon fibre reinforced PEEK composites, Composites Science and technology. 35 (1989) 31-51.

[24] K. Friedrich, T. Gogeva and S. Fakirov, Thermoplastic impregnated fiber bundles: Manufacturing of laminates and fracture mechanics characterization, Composites Science and technology. 33 (1988) 97-120.

[25] N. S. Choi, H. Yamaguchi and K. Takahashi,

Fracture behavior of unidirectional commingled-yarn based carbon fiber/polymide 6 under three-point bending, Journal of Composite Materials. 30 (1996) 760-784.

[26] J. G. Williams, Fracture Mechanics of Polymers, Ellis Hollywood Limited, Halsted Press, (1987).

[27] M. Kawai, A. Hachinohe, K. Takumida and Y. Kawase. Off-Axis Fatigue Behaviour and Its Damage Mechanics Modelling for Unidirectional Fibre Metal Hybrid Composite: GLARE 2, Composite: GLARE 2, Composites Part A. 32 (2001) 13-23.